optica

Self-homodyne-enabled generation of indistinguishable photons

Kai Müller,† Kevin A. Fischer,† Constantin Dory,† Tomas Sarmiento, Konstantinos G. Lagoudakis, Armand Rundquist, Yousif A. Kelaita, and Jelena Vučković*

E. L. Ginzton Laboratory, Stanford University, Stanford, California 94305, USA
**Corresponding author: jela@stanford.edu*

Received 26 April 2016; revised 27 June 2016; accepted 2 August 2016 (Doc. ID 264070); published 23 August 2016

The rapid generation of non-classical light serves as the foundation for exploring quantum optics and developing applications such as secure communications or the generation of NOON states. While strongly coupled quantum dot-photonic crystal resonator systems have great potential as non-classical light sources due to their promise of tailored output statistics, the generation of indistinguishable photons has been obscured due to the strongly dissipative nature of such systems. Here, we demonstrate that the recently discovered self-homodyne suppression technique can be used to overcome this limitation and tune the quantum statistics of transmitted light, achieving indistinguishable photon emission competitive with state-of-the-art metrics. Furthermore, our nanocavity-based platform directly lends itself to scalable on-chip architectures for quantum information.

OCIS codes: (270.5580) Quantum electrodynamics; (270.5290) Photon statistics.

http://dx.doi.org/10.1364/OPTICA.3.000931

1. INTRODUCTION

Understanding the interaction between light and matter is of paramount importance for exploring the peculiar properties of quantum optics and utilizing them for applications such as non-classical light generation with implications for communications, information processing, and sensing [1–5]. In the solid state, self-assembled quantum dots (QDs) are widely used as quantum emitters due to their strong interaction with light and their ability to be integrated into nanophotonic resonators for enhanced light-matter interactions. Examples of quantum optical landmark experiments with QDs are the generation of indistinguishable photons [6–11], entangled photon pairs [12–15], and the observation of Mollow triplets [16,17].

For off-chip applications, a high photon extraction efficiency is desirable, which can be achieved by embedding the QD into a resonator with strong vertical emission. For example, QDs have been embedded in micropillar cavities [6,7] that also Purcell enhance the emission rate for fast photon extraction. Utilizing the resonant excitation of such structures, highly indistinguishable photon generation has recently been demonstrated [18–20]. Importantly, resonant excitation enables a high degree of indistinguishability due to the absence of excitation timing jitter and electric field noise that typically results from charge fluctuations in the semiconductor environment under non-resonant excitation [8,9].

On the other hand, for on-chip applications, photonic crystal resonators are promising. Their planar geometry naturally allows for coupling with on-chip structures, including waveguides and on-chip detectors [21,22], and hence holds promise to realize fully integrated quantum optical hardware. Photonic crystal resonators provide extremely small mode volumes that enable a large enhancement of the light-matter interaction strength with embedded quantum emitters [23–25]. Importantly, in transmission geometries on-chip resonant generation of non-classical light cannot be achieved by resonantly exciting a QD weakly coupled to a resonator. Resonant excitation of a weakly coupled QD-resonator system predominantly leads to coherent scattering from the cavity. Thus, in off-chip applications with micropillars, suppressing this coherent scattering while collecting emissions from the QD using cross-polarized suppression is only enabled by the careful choice of a quantum emitter structure. Specifically, the structure must allow that the polarization of the coherently scattered light is not rotated while the polarization of the QD emission is rotated. This can be achieved, for example, in bi-modal cavities and charge-neutral QDs that have their symmetry axis different from the cavity and laser [26] or bi-modal cavities and charged QDs. Instead, in photonic crystals, direct transmission of light through a strongly coupled QD-nanocavity system can generate a range of output quantum statistics [27–31]. However, the strongly dissipative nature of such systems has so far obscured the generation of indistinguishable photons.

In this paper, we demonstrate that interference, which is intrinsic to photonic crystal cavities, can be used to overcome this strongly dissipative nature and tune quantum statistics. Specifically, we show that this recently discovered self-homodyne suppression (SHS) effect [32] can be used to interferometrically reject the coherent scattering off a dissipative Jaynes–Cummings (JC) system and isolate the non-classical component of the emitted light. While our experimental approach is tailored to photonic

crystal cavities, self-homodyne suppression as a tool for engineering quantum statistics is widely applicable to other JC systems. Here, we demonstrate the robust and ultrafast generation of highly indistinguishable photons from strongly coupled quantum dot-photonic crystal resonator systems with state-of-the-art indistinguishability and generation rates. Additionally, this approach circumvents the temperature limit, set by phonon dephasing, in all previous solid-state approaches [6,10,11] while also facilitating on-chip integration.

2. EXPERIMENT

The system under investigation consists of a single self-assembled quantum dot strongly coupled to a photonic crystal L3 cavity [Fig. 1(a)]. The resulting energy level structure is well described by the JC dressed states ladder. The energies of the lowest two rungs are presented in Fig. 1(b) as a function of the QD-cavity detuning Δ. They form pairs of anticrossing lines, labeled UPn and LPn, for the upper and lower polaritons of rung n, respectively. Experimentally, this coupling can be observed in detuning-dependent cross-polarized reflectivity measurements [Fig. 1(c)] that reveal the clear anticrossing of the first rung [33]. As the polaritonic peaks transition through the avoided crossing (at $\Delta = 0$), they change characters from cavity/QD-like to QD/cavity-like.

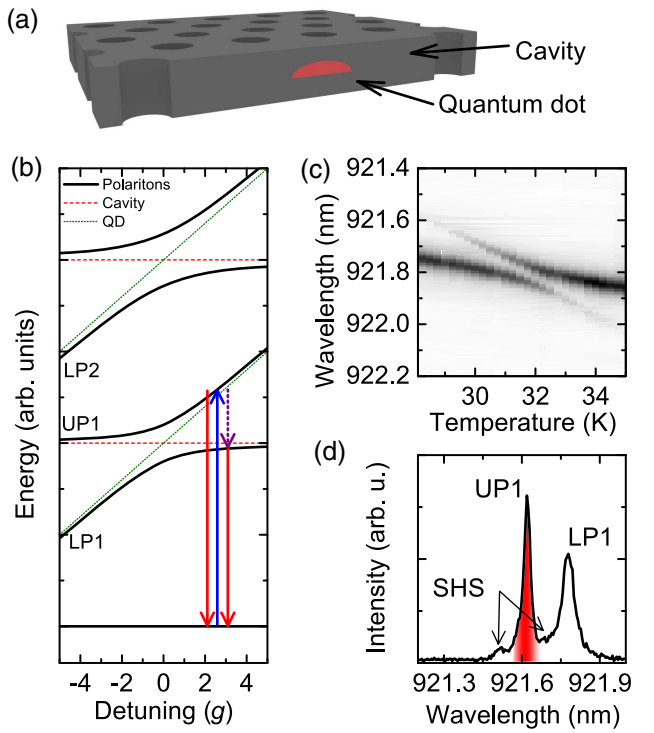

Fig. 1. Resonantly excited strongly coupled system. (a) Schematic illustration of the QD-photonic crystal cavity platform. (b) Schematic illustration of the Jaynes–Cummings (JC) ladder of dressed states that describes the energy level structure of a strongly coupled system. The arrows illustrate the resonant excitation of UP1 and subsequent relaxation. (c) Cross-polarized reflectivity spectrum of the coupled quantum dot-cavity system obtained by temperature tuning the QD through the cavity resonance. An anticrossing of the peaks clearly demonstrates the strong coupling. (d) Typical spectrum for resonantly exciting UP1 with a 16 ps long pulse at a QD-cavity detuning of $\Delta = 4.5g$ and in the presence of self-homodyne suppression. The red shaded region indicates the spectral filter used in subsequent experiments.

Fitting the data results in a QD-cavity coupling strength of $g = 2\pi \cdot 12.3$ GHz and a cavity energy decay rate of $\kappa = 2\pi \cdot 18.4$ GHz.

Resonant generation of single photons in such systems can be achieved by photon blockade [27]. Here, an excitation laser tuned in resonance with the first rung is out of resonance with higher climbs up the ladder due to the JC anharmonicity. However, these resonances have broad linewidths and hence appreciable overlap due to the highly dissipative character of semiconducting systems. Nevertheless, by detuning the QD and cavity by a few g and exciting the QD-like polariton branch, high purity and efficiency single-photon generation has recently been demonstrated [blue arrow in Fig. 1(b)] [30]. To achieve the strongest photon blockade in pulsed on-demand applications, the pulse length has to be chosen as a compromise that minimizes both re-excitation and resonance overlap [31].

We now discuss photon blockades in the context of self-homodyne suppression. Here, the suppression results from destructive interference between the light scattered from the fundamental cavity mode and the continuum above-the-light-line modes, leading to Fano-like resonances [34]. This effect can be used to significantly suppress the JC coherent scattering of the excitation laser in detuned QD-cavity systems and extract the incoherent spectrum [32]. To reach SHS, we optimized the excitation conditions (focus and polarization) for the suppression of coherent scattering. The pulse length is chosen to be only 16 ps to minimize re-excitation. The resulting spectrum [Fig. 1(d)] exhibits three distinct features: emission from the resonantly excited QD-like UP1, phonon-assisted emission from the cavity-like LP1 [purple and red arrows in Fig. 1(b)], and self-homodyne suppressed JC coherently scattered laser light. The last one is strongest on the sides of the UP1 peak due to the spectral dependence of SHS that results from the wavelength-dependent phase shift of the JC coherently scattered light.

To investigate the single-photon generation and photon indistinguishability under resonant excitation of UP1 [Fig. 1(d)], we measure photon correlations between the outputs of a fiber-based Mach–Zehnder (MZ) interferometer [Fig. 2(a)]. Here, we excite the system with double pulses that each have a pulse area of π (see Supplement 1) and a time delay $T_1 = 1.9$ ns that matches the delay of the interferometer. First, we perform experiments without spectral filtering. The result [Fig. 2(b)] is a pattern of five peaks separated by T_1 and repeated with the repetition rate of the laser (80 MHz). Due to the quantum character of the emission, the three center peaks around zero time delay are attenuated [6]. Note that the asymmetry of the five peaks results from the imperfect reflectivity to transmittivity ratios of the second beam splitter in the fiber-coupled implementation (see Supplement 1 for details). To quantitatively analyze the data, we bin the counts in a time window of 384 ps about the peaks [Fig. 2(b) data points]. A fit to the data [blue columns in Fig. 2(c)] allows for extraction of the measured degree of second-order coherence $g^{(2)}[0]$ and first-order coherence $|g^{(1)}[0]|$ between two subsequent pulses. The extracted values of the fit are $g^{(2)}[0] = 0.24 \pm 0.03$ and $|g^{(1)}[0]|^2 = 0.25 \pm 0.03$. In the literature, when analyzing the attenuation of the center peak instead of $|g^{(1)}[0]|^2$, a quantity v is often stated and defined as the single-photon mode overlap. However, this parameter v would only correspond to the single-photon mode overlap for pulses of perfect single-photon character ($g^{(2)}[0] = 0$). The limited fidelity of the measurement can be understood by recalling the emission spectrum presented

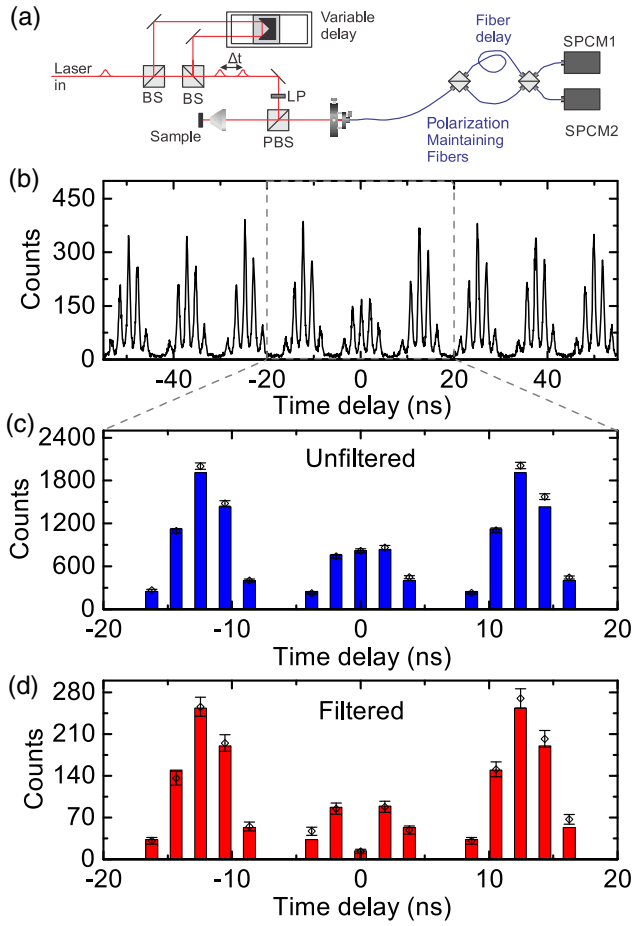

Fig. 2. Indistinguishability measurements. (a) Schematic illustration of the setup used to extract Hong–Ou–Mandel interference. (b) Measured correlation function of the emission using the same excitation conditions as in Fig. 1(d). Due to the quantum character of the light, the amplitude of the three center peaks surrounding zero time delay is reduced. (c) Amplitudes around zero delay obtained from binning the data presented in (b) with a temporal width of 384 ps about the center of each peak (represented as diamond data points). The error bars result from the $\sqrt{N}$ variation of the photocount distribution. Fits to the data are presented as blue columns and reveal $g^{(2)}[0] = 0.24 \pm 0.03$ and $|g^{(1)}[0]|^2 = 0.25 \pm 0.03$. (d) Same as (c) but under spectral filtering of the emission from UP1, resulting in $g^{(2)}[0] = 0.05 \pm 0.04$ and $|g^{(1)}[0]|^2 = 0.96 \pm 0.05$.

in Fig. 1(d). The imperfect suppression of the JC coherently scattered light limits $g^{(2)}[0]$, while the phonon-assisted emission from LP1 limits $|g^{(1)}[0]|^2$ due to excitation timing jitter.

To increase the fidelity of indistinguishable photon generation through photon blockade, we now employ spectral filtering. Therefore, we repeat the correlation measurement while filtering on the UP1 emission, as indicated by the red shaded region in Fig. 1(d). The result of this experiment with a filter bandwidth of $2\pi \cdot 10$ GHz is presented in Fig. 2(d) as empty diamonds. A fit (red columns) extracts values of $g^{(2)}[0] = 0.05 \pm 0.04$ and $|g^{(1)}[0]|^2 = 0.96 \pm 0.05$. Note that this bandwidth is much larger than the linewidth of the UP1 emission. Therefore, the improvements result only from eliminating imperfect suppressions of JC coherently scattered light and phonon-assisted emission from LP1 and not from filtering with a bandwidth smaller than the spectral diffusion of the QD. In both cases, frequency filtered and unfiltered, we confirmed the extracted values of $g^{(2)}[0]$ in second-order correlation measurements and obtained similar values. Our metrics are competitive with the best values obtained from QDs so far [8,9,18,19]. The UP1 state lifetime in our experiment of 55 ps (measured at this detuning [31]) paves the way for on-chip generation rates over an order of magnitude faster than bulk QDs and slightly faster than those in micropillar resonators [18–20]. However, micropillar resonators are optimized for photon extraction, leading to higher count rates, and they also do not require spectral filtering. Nevertheless, as discussed above, the photonic crystal platform facilitates scalable on-chip architectures, and in this platform, its near-unity coupling efficiency to waveguides matters over its emission profile. Finally, the measurements presented here have been performed at a relatively high temperature of approximately 30 K, directly contrasting with the best previously reported Hong–Ou–Mandel (HOM) interference visibility of <40% at such a temperature [11]. This difference can be understood from the interaction with the high-temperature phonon bath: in bulk, the interaction with phonons results in dephasing the emission, which reduces the first-order coherence. Meanwhile, in a strongly coupled system, the interaction with phonons leads to a population transfer from UP1 to LP1 [31], spectrally removing the dephased emission from the detection channel and ensuring a robust, high-fidelity operation. Thus, we have investigated indistinguishable photon generation in a dephasing regime unlike all previous experiments and found that this region is highly beneficial for photon indistinguishability.

3. THEORY

To corroborate our finding that the combination of SHS and spectral filtering results in high-fidelity generation of indistinguishable photons, we performed quantum optical simulations (see Supplement 1). The simulated emission spectrum using the measured system parameters and excitation with a π pulse is presented in Fig. 3(a) without (blue) and with optimized (black) SHS (see Supplement 1 for details). Only when it includes SHS is the spectrum in extremely good qualitative agreement with the experimentally measured one. To demonstrate the impact of SHS on the single-photon character of the emission, we simulate $g^{(2)}[0]$ as a function of the SHS strength without [Fig. 3(b) black] and with [Fig. 3(b) red] spectral filtering of the emission from UP1. Here, the parameter α denotes the intensity of the continuum-mode scattered contribution. In both cases, a clear dip in the values of $g^{(2)}[0]$ very close to the measured values is obtained, with much lower $g^{(2)}[0]$ for the filtered system. Moreover, at the point of best suppression, the simulations reveal that the average number of photons exiting the system per pulse is unity.

To investigate photon indistinguishability, we calculate the second-order cross correlation $g^{(2)}_{\mathrm{HOM}}[0]$ discussed in the original HOM paper [35]. Here, correlations between the output ports of a beam splitter are simulated while two identical systems feed the input ports. It is important to note that in contrast to the often-confused statements in the literature, in this configuration, the dip in the correlation $g^{(2)}_{\mathrm{HOM}}[0]$ is different from the dip of the center peak of the Fig. 2(a) MZ implementation (see Supplement 1 for details). This distinction is important because the MZ scheme is now predominantly used to experimentally characterize single-photon source indistinguishability in our and other experiments. Here, an important result of our work is that the HOM configuration shows a dip of

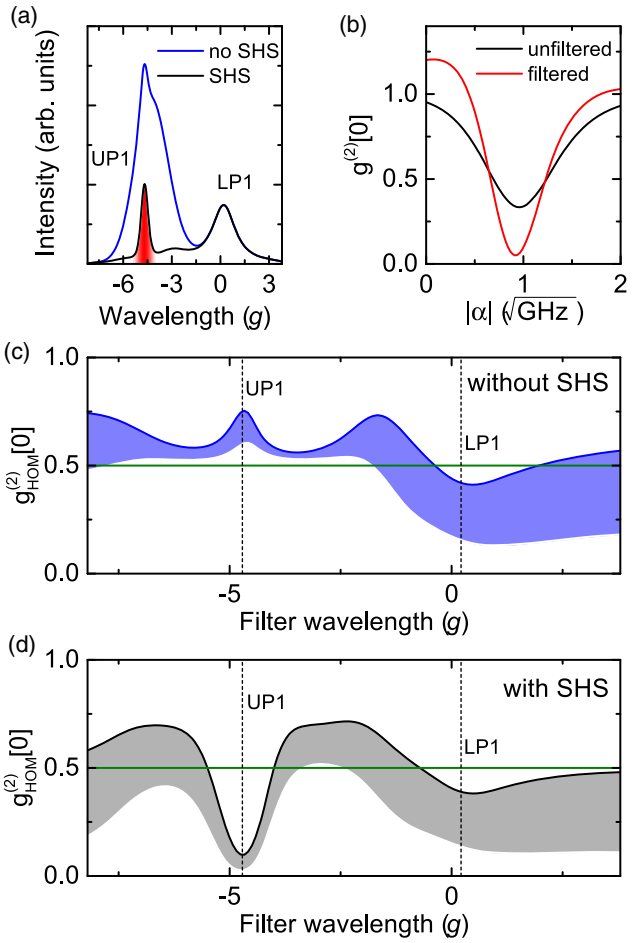

Fig. 3. Quantum optical simulations. (a) Simulated spectrum for resonant excitation of UP1 by a 16 ps long π pulse at a QD-cavity detuning $\Delta = 4.5g$, with and without SHS. (b) $g^{(2)}[0]$ (second-order coherence) for the excitation conditions of (a) (resonant excitation of UP1) as a function of the SHS tuning parameter with and without spectral filtering on UP1 (red region in (a). (c, d) $g^{(2)}_{\mathrm{HOM}}[0]$ as a function of the filtering wavelength excluding (c) and including (d) SHS. Only the central wavelength of the filter changes, but bandwidth remains the same. The shaded area below the curves visualizes $\frac{1}{2}(1 - |g^{(1)}[0]|^2)$, while the white area visualizes $\frac{1}{2}g^{(2)}[0]$. Green lines denote the non-classical threshold. All wavelengths are referenced to that of the bare cavity.

$$g^{(2)}_{\mathrm{HOM}}[0] = \frac{1}{2}g^{(2)}[0] + \frac{1}{2}[1 - |g^{(1)}[0]|^2], \quad (1)$$

while the MZ zero delay dip reduces to

$$g^{(2)}_{\mathrm{MZ}}[0] = \frac{2}{3}g^{(2)}[0] + \frac{1}{3}[1 - |g^{(1)}[0]|^2]. \quad (2)$$

Therefore, the two are equal only for $g^{(2)}[0] = 0$ and $g^{(1)}[0] = 1$. To visualize this difference, we look at our experimentally obtained values of $g^{(2)}[0]$ and $|g^{(1)}[0]|^2$ discussed above. For the frequency filtered case, we obtain $g^{(2)}_{\mathrm{HOM}}[0] = 0.045 \pm 0.045$ and $g^{(2)}_{\mathrm{MZ}}[0] = 0.047 \pm 0.043$, while for the unfiltered case, we obtain $g^{(2)}_{\mathrm{HOM}}[0] = 0.495 \pm 0.03$ and $g^{(2)}_{\mathrm{MZ}}[0] = 0.41 \pm 0.03$. In the filtered case, the difference is small due to the comparable values of $g^{(2)}[0]$ and $1 - |g^{(1)}[0]|^2$, but in the unfiltered case, the difference is significant. Nevertheless, when extracting $g^{(2)}[0]$ and $|g^{(1)}[0]|^2$, it is possible to directly compare the values obtained from the two different methods, as well as the simulations and experiment.

The results of the HOM simulations are presented in Figs. 3(c) and 3(d), excluding and including SHS, respectively. The figures show $g^{(2)}_{\mathrm{HOM}}[0]$ against the filtering wavelength as solid lines. The area below the line is decomposed into $\frac{1}{2}(1 - |g^{(1)}[0]|^2)$ (shaded) and $\frac{1}{2}g^{(2)}[0]$ (white). Without SHS, only a weak dip at the wavelength of LP1 is observed. However, it is barely non-classical since at this wavelength, the emission is phonon mediated and, thus, subject to strong excitation timing jitter, which is reflected in the low value of $|g^{(1)}[0]|^2$. In contrast, when including SHS, a strong dip at the filtered wavelength of UP1 is observed with values of $g^{(2)}[0] = 0.05$ and $|g^{(1)}[0]|^2 = 0.86$, in excellent agreement with the experimentally measured values.

4. CONCLUSION

In summary, we have demonstrated that the self-homodyne technique can be used to interferometrically tune the output quantum statistics of JC systems. In particular, we showed that strongly coupled QD-photonic crystal nanocavity systems are capable of robust and high-fidelity generation of indistinguishable photons even at elevated temperatures by combining resonant excitation, self-homodyne suppression, and spectral filtering. Having produced indistinguishable photons from a state with a lifetime of only 55 ps, our results could pave the way for sources with unprecedented rates. Moreover, the short lifetime leads to a homogeneous linewidth of the emission, which is much larger than that of bulk QDs. Therefore, we expect the indistinguishability to be unaffected by the spectral diffusion of the quantum emitter even without active suppression of the spectral diffusion [36–38]. Specifically, in contrast to bulk QDs [8,11], we expect a similarly high indistinguishability for excitation pulses with a longer time delay or for measurements interfering the emission from multiple systems. Furthermore, the generation of indistinguishable photons from strongly coupled QD-photonic crystal systems enables scalable on-chip architectures. While in our case the positioning of the QD relative to the cavity has been done probabilistically, recent progress in site-selective growth of QDs [39,40] as well as positioning of resonators relative to QDs [10,18,20] provides further support for the feasibility of integrated quantum photonic circuits. Finally, the demonstration of the self-homodyne technique to isolate the quantum character of resonantly scattered light paves the way for photon bundling [29] at significantly lower nonlinearity cavity detunings and smaller powers for the high-throughput generation of other non-classical states of light.

Funding. Air Force Office of Scientific Research (AFOSR) MURI Center for Multifunctional Light-Matter Interfaces Based on Atoms and Solids (FA9550-12-1-0025); Army Research Office (ARO) (W911NF1310309); National Science Foundation (NSF) Division of Materials Research (DMR) (1503759); Alexander von Humboldt Foundation; Schweizerischer Nationalfonds zur Förderung der Wissenschaftlichen Forschung (SNF).

Acknowledgment. K. M. acknowledges support from the Alexander von Humboldt Foundation. K. A. F. acknowledges support from the Lu Stanford Graduate Fellowship and the National Defense Science and Engineering Graduate Fellowship. C. D. acknowledges support from the Stanford Graduate

Fellowship. K. G. L. acknowledges support from the Swiss National Science Foundation. Y. A. K. acknowledges support from the Stanford Graduate Fellowship and the National Defense Science and Engineering Graduate Fellowship.

†These authors contributed equally to this work.

See Supplement 1 for supporting content.

REFERENCES

1. N. Gisin, G. Ribordy, W. Tittel, and H. Zbinden, "Quantum cryptography," Rev. Mod. Phys. **74**, 145–195 (2002).
2. N. Gisin and R. Thew, "Quantum communication," Nat. Photonics **1**, 165–171 (2007).
3. J. L. O'Brien, "Optical quantum computing," Science **318**, 1567–1570 (2007).
4. A. N. Boto, P. Kok, D. S. Abrams, S. L. Braunstein, C. P. Williams, and J. P. Dowling, "Quantum interferometric optical lithography: exploiting entanglement to beat the diffraction limit," Phys. Rev. Lett. **85**, 2733–2736 (2000).
5. V. Giovannetti, S. Lloyd, and L. Maccone, "Quantum-enhanced measurements: beating the standard quantum limit," Science **306**, 1330–1336 (2004).
6. C. Santori, D. Fattal, J. Vučković, G. S. Solomon, and Y. Yamamoto, "Indistinguishable photons from a single-photon device," Nature **419**, 594–597 (2002).
7. O. Gazzano, S. Michaelis de Vasconcellos, C. Arnold, A. Nowak, E. Galopin, I. Sagnes, L. Lanco, A. Lemaître, and P. Senellart, "Bright solid-state sources of indistinguishable single photons," Nat. Commun. **4**, 1425 (2013).
8. Y.-M. He, Y. He, Y.-J. Wei, D. Wu, M. Atature, C. Schneider, S. Hofling, M. Kamp, C.-Y. Lu, and J.-W. Pan, "On-demand semiconductor single-photon source with near-unity indistinguishability," Nat. Nanotechnol. **8**, 213–217 (2013).
9. Y.-J. Wei, Y.-M. He, M.-C. Chen, Y.-N. Hu, Y. He, D. Wu, C. Schneider, M. Kamp, S. Höfling, C.-Y. Lu, and J.-W. Pan, "Deterministic and robust generation of single photons from a single quantum dot with 99.5% indistinguishability using adiabatic rapid passage," Nano Lett. **14**, 6515–6519 (2014).
10. M. Gschrey, A. Thoma, P. Schnauber, M. Seifried, R. Schmidt, B. Wohlfeil, L. Kruger, J. H. Schulze, T. Heindel, S. Burger, F. Schmidt, A. Strittmatter, S. Rodt, and S. Reitzenstein, "Highly indistinguishable photons from deterministic quantum-dot microlenses utilizing three-dimensional *in situ* electron-beam lithography," Nat. Commun. **6**, 7662 (2015).
11. A. Thoma, P. Schnauber, M. Gschrey, M. Seifried, J. Wolters, J.-H. Schulze, A. Strittmatter, S. Rodt, A. Carmele, A. Knorr, T. Heindel, and S. Reitzenstein, "Exploring dephasing of a solid-state quantum emitter via time- and temperature-dependent Hong-Ou-Mandel experiments," Phys. Rev. Lett. **116**, 033601 (2016).
12. O. Benson, C. Santori, M. Pelton, and Y. Yamamoto, "Regulated and entangled photons from a single quantum dot," Phys. Rev. Lett. **84**, 2513–2516 (2000).
13. N. Akopian, N. H. Lindner, E. Poem, Y. Berlatzky, J. Avron, D. Gershoni, B. D. Gerardot, and P. M. Petroff, "Entangled photon pairs from semiconductor quantum dots," Phys. Rev. Lett. **96**, 130501 (2006).
14. R. Trotta, J. S. Wildmann, E. Zallo, O. G. Schmidt, and A. Rastelli, "Highly entangled photons from hybrid piezoelectric-semiconductor quantum dot devices," Nano Lett. **14**, 3439–3444 (2014).
15. M. Müller, S. Bounouar, K. D. Jöns, M. Glässl, and P. Michler, "On-demand generation of indistinguishable polarization-entangled photon pairs," Nat. Photonics **8**, 224–228 (2014).
16. A. Nick Vamivakas, Y. Zhao, C.-Y. Lu, and M. Atature, "Spin-resolved quantum-dot resonance fluorescence," Nat. Phys. **5**, 198–202 (2009).
17. E. B. Flagg, A. Muller, J. W. Robertson, S. Founta, D. G. Deppe, M. Xiao, W. Ma, G. J. Salamo, and C. K. Shih, "Resonantly driven coherent oscillations in a solid-state quantum emitter," Nat. Phys. **5**, 203–207 (2009).
18. N. Somaschi, V. Giesz, L. De Santis, J. C. Loredo, M. P. Almeida, G. Hornecker, S. L. Portalupi, T. Grange, C. Antón, J. Demory, C. Gómez, I. Sagnes, N. D. Lanzillotti-Kimura, A. Lematre, A. Auffeves, A. G. White, L. Lanco, and P. Senellart, "Near-optimal single-photon sources in the solid state," Nat. Photonics **10**, 340–345 (2016).
19. X. Ding, Y. He, Z.-C. Duan, N. Gregersen, M.-C. Chen, S. Unsleber, S. Maier, C. Schneider, M. Kamp, S. Höfling, C.-Y. Lu, and J.-W. Pan, "On-demand single photons with high extraction efficiency and near-unity indistinguishability from a resonantly driven quantum dot in a micropillar," Phys. Rev. Lett. **116**, 020401 (2016).
20. S. Unsleber, Y.-M. He, S. Gerhardt, S. Maier, C.-Y. Lu, J.-W. Pan, N. Gregersen, M. Kamp, C. Schneider, and S. Höfling, "Highly indistinguishable on-demand resonance fluorescence photons from a deterministic quantum dot micropillar device with 74% extraction efficiency," Opt. Express **24**, 8539–8546 (2016).
21. G. Reithmaier, S. Lichtmannecker, T. Reichert, P. Hasch, K. Muller, M. Bichler, R. Gross, and J. J. Finley, "On-chip time resolved detection of quantum dot emission using integrated superconducting single photon detectors," Sci. Rep. **3**, 1901 (2013).
22. G. Reithmaier, M. Kaniber, F. Flassig, S. Lichtmannecker, K. Müller, A. Andrejew, J. Vučković, R. Gross, and J. J. Finley, "On-chip generation, routing, and detection of resonance fluorescence," Nano Lett. **15**, 5208–5213 (2015).
23. T. Yoshie, A. Scherer, J. Hendrickson, G. Khitrova, H. M. Gibbs, G. Rupper, C. Ell, O. B. Shchekin, and D. G. Deppe, "Vacuum Rabi splitting with a single quantum dot in a photonic crystal nanocavity," Nature **432**, 200–203 (2004).
24. D. Englund, D. Fattal, E. Waks, G. Solomon, B. Zhang, T. Nakaoka, Y. Arakawa, Y. Yamamoto, and J. Vučković, "Controlling the spontaneous emission rate of single quantum dots in a two-dimensional photonic crystal," Phys. Rev. Lett. **95**, 013904 (2005).
25. K. Hennessy, A. Badolato, M. Winger, D. Gerace, M. Atatüre, S. Gulde, S. Fält, E. L. Hu, and A. Imamoğlu, "Quantum nature of a strongly coupled single quantum dot-cavity system," Nature **445**, 896–899 (2007).
26. V. Giesz, N. Somaschi, G. Hornecker, T. Grange, B. Reznychenko, L. De Santis, J. Demory, C. Gomez, I. Sagnes, A. Lemaitre, O. Krebs, N. D. Lanzillotti-Kimura, L. Lanco, A. Auffeves, and P. Senellart, "Coherent manipulation of a solid-state artificial atom with few photons," Nat. Commun. **7**, 11986 (2016).
27. A. Faraon, I. Fushman, D. Englund, N. Stoltz, P. Petroff, and J. Vuckovic, "Coherent generation of non-classical light on a chip via photon-induced tunnelling and blockade," Nat. Phys. **4**, 859–863 (2008).
28. A. Reinhard, T. Volz, M. Winger, A. Badolato, K. J. Hennessy, E. L. Hu, and A. Imamoglu, "Strongly correlated photons on a chip," Nat. Photonics **6**, 93–96 (2011).
29. C. S. Muñoz, E. del Valle, A. G. Tudela, K. Müller, S. Lichtmannecker, M. Kaniber, C. Tejedor, J. J. Finley, and F. P. Laussy, "Emitters of N-photon bundles," Nat. Photonics **8**, 550–555 (2014).
30. K. Müller, A. Rundquist, K. A. Fischer, T. Sarmiento, K. G. Lagoudakis, Y. A. Kelaita, C. Sánchez Muñoz, E. del Valle, F. P. Laussy, and J. Vučković, "Coherent generation of nonclassical light on chip via detuned photon blockade," Phys. Rev. Lett. **114**, 233601 (2015).
31. K. Müller, K. A. Fischer, A. Rundquist, C. Dory, K. G. Lagoudakis, T. Sarmiento, Y. A. Kelaita, V. Borish, and J. Vučković, "Ultrafast polariton-phonon dynamics of strongly coupled quantum dot-nanocavity systems," Phys. Rev. X **5**, 031006 (2015).
32. K. A. Fischer, K. Müller, A. Rundquist, T. Sarmiento, A. Y. Piggott, Y. Kelaita, C. Dory, K. G. Lagoudakis, and J. Vučković, "Self-homodyne measurement of a dynamic mollow triplet in the solid state," Nat. Photonics **10**, 163–166 (2016).
33. D. Englund, A. Faraon, I. Fushman, N. Stoltz, P. Petroff, and J. Vuckovic, "Controlling cavity reflectivity with a single quantum dot," Nature **450**, 857–861 (2007).
34. J. P. Vasco, H. Vinck-Posada, P. T. Valentim, and P. S. S. Guimãraes, "Modeling of fano resonances in the reflectivity of photonic crystal cavities with finite spot size excitation," Opt. Express **21**, 31336–31346 (2013).
35. C. K. Hong, Z. Y. Ou, and L. Mandel, "Measurement of subpicosecond time intervals between two photons by interference," Phys. Rev. Lett. **59**, 2044–2046 (1987).
36. J. H. Prechtel, A. V. Kuhlmann, J. Houel, L. Greuter, A. Ludwig, D. Reuter, A. D. Wieck, and R. J. Warburton, "Frequency-stabilized source of single photons from a solid-state qubit," Phys. Rev. X **3**, 041006 (2013).
37. J. Hansom, C. H. H. Schulte, C. Matthiesen, M. J. Stanley, and M. Atatüre, "Frequency stabilization of the zero-phonon line of a quantum

dot via phonon-assisted active feedback," Appl. Phys. Lett. **105**, 172107 (2014).
38. A. V. Kuhlmann, J. H. Prechtel, J. Houel, A. Ludwig, D. Reuter, A. D. Wieck, and R. J. Warburton, "Transform-limited single photons from a single quantum dot," Nat. Commun. **6**, 8204 (2015).
39. M. K. Yakes, L. Yang, A. S. Bracker, T. M. Sweeney, P. G. Brereton, M. Kim, C. S. Kim, P. M. Vora, D. Park, S. G. Carter, and D. Gammon, "Leveraging crystal anisotropy for deterministic growth of InAs quantum dots with narrow optical linewidths," Nano Lett. **13**, 4870–4875 (2013).
40. S. Unsleber, S. Maier, D. P. S. McCutcheon, Y.-M. He, M. Dambach, M. Gschrey, N. Gregersen, J. Mørk, S. Reitzenstein, S. Höfling, C. Schneider, and M. Kamp, "Observation of resonance fluorescence and the mollow triplet from a coherently driven site-controlled quantum dot," Optica **2**, 1072–1077 (2015).